

Decoherence effect on Fano line shapes in double quantum dots coupled between normal and superconducting leads

J. Barański and T. Domański

Institute of Physics, M. Curie-Skłodowska University, 20-031 Lublin, Poland

(Received 15 March 2012; published 29 May 2012)

We investigate the Fano-type spectroscopic line shapes of the T-shape double quantum dot coupled between the conducting and superconducting electrodes and analyze their stability on a decoherence. Because of the proximity effect the quantum interference patterns appear simultaneously at $\pm\varepsilon_2$, where ε_2 is an energy of the side-attached quantum dot. We find that decoherence gradually suppresses both such interferometric structures. We also show that at low temperatures another tiny Fano-type structure can be induced upon forming the Kondo state on the side-coupled quantum dot due to its coupling to the floating lead.

DOI: [10.1103/PhysRevB.85.205451](https://doi.org/10.1103/PhysRevB.85.205451)

PACS number(s): 73.63.Kv, 73.23.Hk, 74.45.+c, 74.50.+r

I. INTRODUCTION

When nanoscopic objects such as quantum dots, nanowires, or thin metallic layers are placed in a neighborhood of superconducting material they partly absorb its order parameter. On a microscopic level this proximity effect causes electrons near the Fermi energy to become bound into pairs. Upon forming a circuit with external leads (which can be chosen as conducting, ferromagnetic, or superconducting) such effect can induce a number of unique properties in the normal and anomalous tunneling channels.¹ For instance, the relation between correlations and the on-dot induced pairing has been recently experimentally probed by the Andreev spectroscopy^{2,3} and the Josephson current measurements⁴⁻⁷ signifying the important role of the Kondo effect on the subgap current.

Here we address the Andreev-type transport through the double quantum dot (DQD) nanostructure coupled between the normal (N) and superconducting (S) leads. We focus on the subgap regime, i.e., energies considerably smaller than the pairing gap Δ of the superconductor. Under such conditions the eigenstates of uncorrelated quantum dots represent either the singly occupied states $|\uparrow\rangle$, $|\downarrow\rangle$ or the coherent superpositions of empty and doubly occupied configurations $u|0\rangle + v|\uparrow\downarrow\rangle$. The effective Bogoliubov-type quasiparticle excitations affect in turn all the spectroscopic features originating, for instance, from the internal structure, the correlations, perturbations, etc. Due to the proximity effect all these features are going to show up *simultaneously* at negative and positive energies.

To highlight this sort of emerging physics we examine in some detail the interference patterns originating from a charge leakage t (assumed to be much weaker than Γ_N and Γ_S) between the central (QD₁) and another side-attached quantum dot (QD₂). We also analyze stability of these patterns with respect to a decoherence induced by the coupling Γ_D to the floating lead (D) as sketched in Fig. 1. Practically this D electrode can be thought as a substrate on which the quantum dots are deposited or can mimic the effects caused by phonons/photons.⁸

The scheme illustrated in Fig. 1 resembles the prototype for a dephasing originally considered (assuming all three leads to be conductors) by Büttiker⁹ and later on by several other authors.^{10,11} The coherent channel represents such electrons which traverse the central quantum dot, moving directly

between N and S electrodes. This coherent part coexists with another (incoherent) current contributed by electrons flowing to the side-attached quantum dot, and scattered by the charge reservoir D . Electrons entering such a fully chaotic fermionic cavity undergo the phase randomization, thereby this tunneling channel is related to the dephasing mechanism. In practical terms any decoherence is expected to suppress the quantum features, therefore stability of the Fano-type interference patterns can be regarded as a useful probe of an interplay between the coherent and incoherent tunneling channels (for more specific argumentation that dephasing is indeed observable via the expectation values; see, e.g., Ref. 12). To estimate the dephasing rate $1/\tau_\phi$ one would need to determine the reduced density matrix $\hat{\rho}(t)$ and investigate the asymptotic exponential decay $\sim e^{-t/\tau_\phi}$ of the off-diagonal terms. The dynamics can be inferred, for instance, from the Bloch-Redfield equations^{13,14} or adopting other real-time methods. Such a nontrivial aspect is, however, beyond the scope of our present study.

In the absence of the floating D electrode the T-shape double quantum dot systems have been already studied considering the case of both metallic leads (see, e.g., Ref. 15) as well as the metallic/superconducting hybrids.¹⁶⁻¹⁸ In the regime of weak interdot coupling t this configuration allows for a realization of the Fano-type line shapes (for a survey on the Fano effect in various systems, see Ref. 19). These features arise when the electron waves are transmitted between the external electrodes via a broad QD₁ spectrum and they happen to interfere with the other electron waves, resonantly scattered on the discrete QD₂ levels.²⁰ Hallmarks of the destructive/constructive quantum interference show up in a form of the asymmetric line shapes $G_0 \frac{(x+q)^2}{x^2+1} + G_1$ in the tunneling conductance, where the dimensionless argument x is proportional to $eV - \varepsilon_2$, q denotes the asymmetry parameter, and $G_{0,1}$ are some background functions slowly varying with respect to V . Such line shapes have been indeed observed experimentally for the DQD coupled between the metallic leads.^{21,22} Similar Fano-type features have been also reported from the spectroscopic measurements for a number of systems, e.g., the cobalt adatoms deposited on Au(111) surfaces,²³ the semiopen nanostructures,^{24,25} the dithiol benzene molecule placed between the gold electrodes,²⁶ the “hidden order” phase of the heavy fermion compound URu₂Si₂,²⁷ the dopant atoms

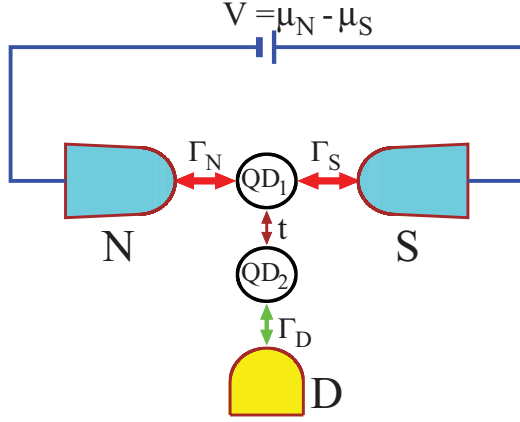


FIG. 1. (Color online) Schematic view of the T-shape double quantum dot coupled to normal (N) and superconducting (S) electrodes and in addition affected by the floating (D) lead that is responsible for a decoherence.

located in the metal near a Schottky barrier metal-oxide-semiconductor field-effect transistor (MOSFET),²⁸ and many others.¹⁹

As far as the proximity effect in N -DQD- S heterojunctions is concerned we have recently emphasized¹⁸ the possibility to observe the particle/hole Fano-type line shapes in the subgap Andreev transport. Here we would like to explore how such Fano-type structures are stable on a decoherence. Since the floating lead (D) does not belong to the closed circuit we assume that a net current to/from such an electrode vanishes, and it merely serves as the source of decoherence. Formally our study extends the previous results of Ref. 8 onto the anomalous Andreev transport. To our knowledge such problem has not been addressed yet in the literature and it might be of practical importance for the experimental measurements. Influence of the bosonic (phonon/photon) modes shall be discussed elsewhere.

In the next section we briefly state formal aspects of the problem. Next, we discuss a changeover of the Fano-type line shapes with respect to the asymmetric coupling Γ_S/Γ_N controlling efficiency of the proximity effect. We also investigate the stability of the particle/hole Fano features with respect to decoherence (in the spectrum and in the Andreev transmittance). Finally, we take into account the correlations. We argue that for strong enough coupling Γ_D the Kondo resonance formed on the side-attached quantum dot QD₂ can induce a tiny interferometric pattern at $\omega = 0$. Such Kondo driven Fano structure could be detectable in the low bias Andreev conductance.

II. THEORETICAL FORMULATION

The double quantum dot nanostructure shown in Fig. 1 can be described by the Anderson impurity Hamiltonian

$$\hat{H} = \hat{H}_{\text{bath}} + \hat{H}_{\text{DQD}} + \hat{H}_T, \quad (1)$$

where the bath $\hat{H}_{\text{bath}} = \sum_{\beta} \hat{H}_{\beta}$ consists of three external charge reservoirs ($\beta = N, S, D$), \hat{H}_{DQD} refers to the double quantum dot, and \hat{H}_T stands for the hybridization part. We treat the conducting leads ($\beta = N, D$) as free Fermi gas

$\hat{H}_{\beta} = \sum_{\mathbf{k}, \sigma} \xi_{\mathbf{k}\beta} \hat{c}_{\mathbf{k}\sigma\beta}^{\dagger} \hat{c}_{\mathbf{k}\sigma\beta}$ and represent the isotropic superconductor by the bilinear BCS form $\hat{H}_S = \sum_{\mathbf{k}, \sigma} \xi_{\mathbf{k}\sigma} \hat{c}_{\mathbf{k}\sigma S}^{\dagger} \hat{c}_{\mathbf{k}\sigma S} - \Delta \sum_{\mathbf{k}} (\hat{c}_{\mathbf{k}\uparrow S}^{\dagger} \hat{c}_{-\mathbf{k}\downarrow S}^{\dagger} + \hat{c}_{-\mathbf{k}\downarrow S} \hat{c}_{\mathbf{k}\uparrow S})$. Using the second quantization $\hat{c}_{\mathbf{k}\sigma\beta}^{(\dagger)}$ denotes the annihilation (creation) operators for spin $\sigma = \uparrow, \downarrow$ electrons in the momentum state \mathbf{k} and the energy $\xi_{\mathbf{k}\beta} = \varepsilon_{\mathbf{k}\beta} - \mu_{\beta}$ measured with respect to the chemical potential μ_{β} .

Following Ref. 8 we assume that the charge transport occurs through the T-shape configuration (Fig. 1) only via the central ($i = 1$) quantum dot, whereas the side-attached QD₂ is responsible for the quantum interference. Hybridization of the quantum dots to the external reservoirs of charge carriers is given by

$$\begin{aligned} \hat{H}_T = & \sum_{\beta=N,S} \sum_{\mathbf{k}, \sigma} (V_{\mathbf{k}\beta} \hat{d}_{1\sigma}^{\dagger} \hat{c}_{\mathbf{k}\sigma\beta} + \text{H.c.}) \\ & + \sum_{\mathbf{k}, \sigma} (V_{\mathbf{k}D} \hat{d}_{2\sigma}^{\dagger} \hat{c}_{\mathbf{k}\sigma D} + \text{H.c.}). \end{aligned} \quad (2)$$

Such couplings indirectly affect both the quantum dots through the interdot hopping t

$$\begin{aligned} \hat{H}_{\text{DQD}} = & \sum_{\sigma, i} \varepsilon_i \hat{d}_{i\sigma}^{\dagger} \hat{d}_{i\sigma} + t \sum_{\sigma} (\hat{d}_{1\sigma}^{\dagger} \hat{d}_{2\sigma} + \text{H.c.}) \\ & + \sum_i U_i \hat{d}_{i\uparrow}^{\dagger} \hat{d}_{i\uparrow} \hat{d}_{i\downarrow}^{\dagger} \hat{d}_{i\downarrow}. \end{aligned} \quad (3)$$

We use standard notation for the annihilation (creation) operators $\hat{d}_i^{(\dagger)}$ for electrons of the quantum dots $i = 1, 2$. The corresponding energy levels are denoted by ε_i and U_i stand for the on-dot Coulomb potential.

Let us emphasize that only the electrodes N and S belong to a closed circuit (as is displayed in Fig. 1), and under nonequilibrium conditions $\mu_N \neq \mu_S$ play a role of the source and sink for the charge current. The third floating lead D can temporarily absorb/reinject electrons, but appropriate tuning of the chemical potential μ_D (Ref. 29) can guarantee that no current would be contributed on average from it. Electrons scattered by such a floating lead experience the inelastic events, leading to their phase randomization. Some quantitative aspects of this dephasing driven by the voltage probe D have been discussed (for the case of conducting electrodes) by a number of authors.⁹⁻¹¹ From the physical point of view, matching the dephased electrons (inelastically scattered by the floating lead) with other electrons (coherently tunneled only through the central quantum dot), the conductance of the resulting total current would reveal their subtle interplay, depending on the magnitude of Γ_D .

For simplicity, we assume that the chemical potentials μ_{β} are safely distant from the band edges and one can impose the wide-band limit approximation, introducing the coupling constants $\Gamma_{\beta} = 2\pi \sum |V_{\mathbf{k}\beta}|^2 \delta(\omega - \xi_{\mathbf{k}\beta})$. We shall use Γ_N as a convenient unit for the energies.

III. PARTICLE-HOLE FANO LINE SHAPES

To account for the proximity effect we have to deal with the mixed particle and hole degrees of freedom. Among the possible ways for doing this one can use the Nambu spinor

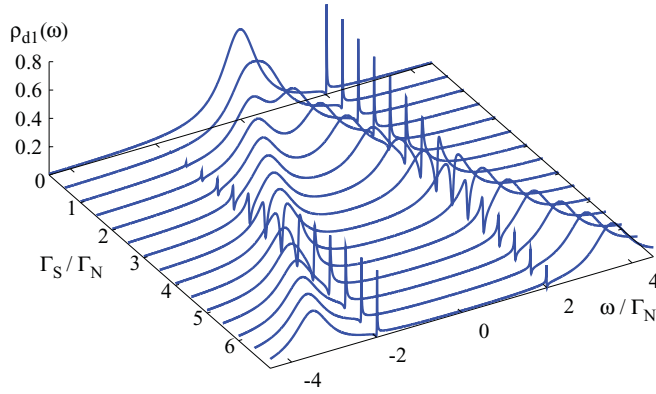


FIG. 2. (Color online) Particle and hole Fano-type line shapes appearing at $\pm\varepsilon_2$ in the spectral function $\rho_{d1}(\omega)$ of the central quantum dot. Calculations are done for the following parameters: $\varepsilon_1 = 0$, $\varepsilon_2 = 2\Gamma_N$, $U_i = 0$, $t = 0.2\Gamma_N$, and $\Delta = 10\Gamma_N$.

notation $\hat{\Psi}_j^\dagger = (\hat{d}_{j\uparrow}^\dagger, \hat{d}_{j\downarrow}^\dagger)$ and $\hat{\Psi}_j = (\hat{\Psi}_j^\dagger)^\dagger$. Spectroscopic and transport properties of the system can be determined from the matrix Green's function $\mathbf{G}_j(t, t_0) = -i\hat{T}\langle\hat{\Psi}_j(t)\hat{\Psi}_j^\dagger(t_0)\rangle$. In the equilibrium case this function depends solely on the time difference $t - t_0$ and its Fourier transform can be expressed by the following Dyson equation:

$$\mathbf{G}_j(\omega)^{-1} = \mathbf{g}_j(\omega)^{-1} - \Sigma_j^0(\omega) - \Sigma_j^{e-e}(\omega), \quad (4)$$

where $\mathbf{g}_j(\omega)$ are the Green's functions of the isolated quantum dots,

$$\mathbf{g}_j(\omega) = \begin{pmatrix} \frac{1}{\omega - \varepsilon_j} & 0 \\ 0 & \frac{1}{\omega + \varepsilon_j} \end{pmatrix}, \quad (5)$$

and the self-energies consist of the noninteracting part $\Sigma_j^0(\omega)$ with the additional correction $\Sigma_j^{e-e}(\omega)$ due to the electron-electron correlations.

Appearance of the particle and hole interference Fano structures (see Fig. 2) can be explained restricting first to the uncorrelated quantum dots. The self-energies $\Sigma_j^0(\omega)$ are given by

$$\Sigma_j^0(\omega) = \sum_{\mathbf{k}, \beta} V_{\mathbf{k}\beta} \mathbf{g}_\beta(\mathbf{k}, \omega) V_{\mathbf{k}\beta}^* + t \mathbf{G}_{j'}(\omega) t^*, \quad (6)$$

where the interdot hopping contribution refers to $j' \neq j$. The Green's functions of the conducting leads $\beta = N, D$ have the diagonal form

$$\mathbf{g}_\beta(\mathbf{k}, \omega) = \begin{pmatrix} \frac{1}{\omega - \xi_{\mathbf{k}\beta}} & 0 \\ 0 & \frac{1}{\omega + \xi_{\mathbf{k}\beta}} \end{pmatrix} \quad (7)$$

whereas the superconducting lead is characterized by the BCS structure

$$\mathbf{g}_S(\mathbf{k}, \omega) = \begin{pmatrix} \frac{u_{\mathbf{k}}^2}{\omega - E_{\mathbf{k}}} + \frac{v_{\mathbf{k}}^2}{\omega + E_{\mathbf{k}}} & \frac{-u_{\mathbf{k}}v_{\mathbf{k}}}{\omega - E_{\mathbf{k}}} + \frac{u_{\mathbf{k}}v_{\mathbf{k}}}{\omega + E_{\mathbf{k}}} \\ \frac{-u_{\mathbf{k}}v_{\mathbf{k}}}{\omega - E_{\mathbf{k}}} + \frac{u_{\mathbf{k}}v_{\mathbf{k}}}{\omega + E_{\mathbf{k}}} & \frac{u_{\mathbf{k}}^2}{\omega + E_{\mathbf{k}}} + \frac{v_{\mathbf{k}}^2}{\omega - E_{\mathbf{k}}} \end{pmatrix} \quad (8)$$

with the corresponding coefficients

$$u_{\mathbf{k}}^2, v_{\mathbf{k}}^2 = \frac{1}{2} \left[1 \pm \frac{\xi_{\mathbf{k}S}}{E_{\mathbf{k}}} \right], \quad u_{\mathbf{k}}v_{\mathbf{k}} = \frac{\Delta}{2E_{\mathbf{k}}},$$

and the quasiparticle energy $E_{\mathbf{k}} = \sqrt{\xi_{\mathbf{k}S}^2 + \Delta^2}$.

In the wide-band limit we obtain for $\beta = N, D$

$$\sum_{\mathbf{k}} V_{\mathbf{k}\beta} \mathbf{g}_\beta(\mathbf{k}, \omega) V_{\mathbf{k}\beta}^* = -i \frac{\Gamma_\beta}{2} \begin{pmatrix} 1 & 0 \\ 0 & 1 \end{pmatrix} \quad (9)$$

and for the superconducting electrode

$$\sum_{\mathbf{k}} V_{\mathbf{k}S} \mathbf{g}_S(\mathbf{k}, \omega) V_{\mathbf{k}S}^* = -i \frac{\Gamma_S}{2} \gamma(\omega) \begin{pmatrix} 1 & \frac{\Delta}{\omega} \\ \frac{\Delta}{\omega} & 1 \end{pmatrix} \quad (10)$$

with

$$\gamma(\omega) = \frac{|\omega| \Theta(|\omega| - \Delta)}{\sqrt{\omega^2 - \Delta^2}} - \frac{i\omega \Theta(\Delta - |\omega|)}{\sqrt{\Delta^2 - \omega^2}}. \quad (11)$$

In a far subgap regime $|\omega| \ll \Delta$ only the off-diagonal terms of the matrix (10) are preserved tending to the static value $-\Gamma_S/2$. This *atomic limit* case has been studied by several groups and the results have been recently summarized in the Ref. 30. For arbitrary Δ we obtain the following set of coupled equations:

$$\mathbf{G}_1(\omega)^{-1} = \left[\omega + i \frac{\Gamma_N + \gamma(\omega)\Gamma_S}{2} \right] \mathbf{I} - \varepsilon_1 \sigma_z + i \frac{\gamma(\omega)\Delta\Gamma_S}{2\omega} \sigma_y - |t|^2 \mathbf{G}_2(\omega), \quad (12)$$

$$\mathbf{G}_2(\omega)^{-1} = \left[\omega + i \frac{\Gamma_D}{2} \right] \mathbf{I} - \varepsilon_2 \sigma_z - |t|^2 \mathbf{G}_1(\omega), \quad (13)$$

where \mathbf{I} stands for the identity matrix and $\sigma_{y,z}$ denote the usual Pauli matrices.

Figure 2 shows the spectral function $\rho_{d1}(\omega)$ obtained in the equilibrium situation for both uncorrelated quantum dots ($U_i = 0$) assuming a weak interdot hopping $t = 0.2\Gamma_N$ (decoherence is not taken into account here). To focus on the subgap regime $|\omega| \ll \Delta$ we used $\Delta = 10\Gamma_N$ and other effects related to the gap edge singularities are separately discussed in the Appendix. For an increasing ratio Γ_S/Γ_N we can notice the following qualitative changes: (a) the initial Lorentzian centered at ε_1 splits into two quasiparticle peaks centered at $\pm E_1 \simeq \pm\sqrt{\varepsilon_1 + (\Gamma_S/2)^2}$ (due to the proximity effect), (b) the usual Fano-type line shape formed at ε_2 is for larger values of Γ_S accompanied by the appearance of its mirror reflection at $-\varepsilon_2$ (we shall refer to these peaks as the particle/hole Fano structures), (c) Fano-type line shapes of these particle/hole features are characterized by an opposite sign of the asymmetry parameter q , (d) the asymmetry parameters exchange the sign for such Γ_S when the quasiparticle energy $\sqrt{\varepsilon_1^2 + (\Gamma_S/2)^2} \sim \varepsilon_2$.

For a closer inspection on the above-mentioned changes we examine in the upper (bottom) panel of Fig. 3 the spectral function $\rho_{d1}(\omega)$ obtained for $\Gamma_S/\Gamma_N = 1.5$ (8) when ε_2 is smaller (larger) than the quasiparticle energy E_1 . We also check the decoherence effect on these particle and hole Fano line shapes. We notice that already a weak coupling Γ_D to the floating lead washes out both these particle and hole Fano structures. Thus we conclude that decoherence has a detrimental effect on the quantum interferometric features. To provide physical argumentation for this behavior let us recall that the resonant level at ε_2 gradually broadens upon increasing Γ_D . For this reason the electron waves are scattered on the side-attached quantum dot without any sharp change of the phase, thereby the Fano-type interference is no longer

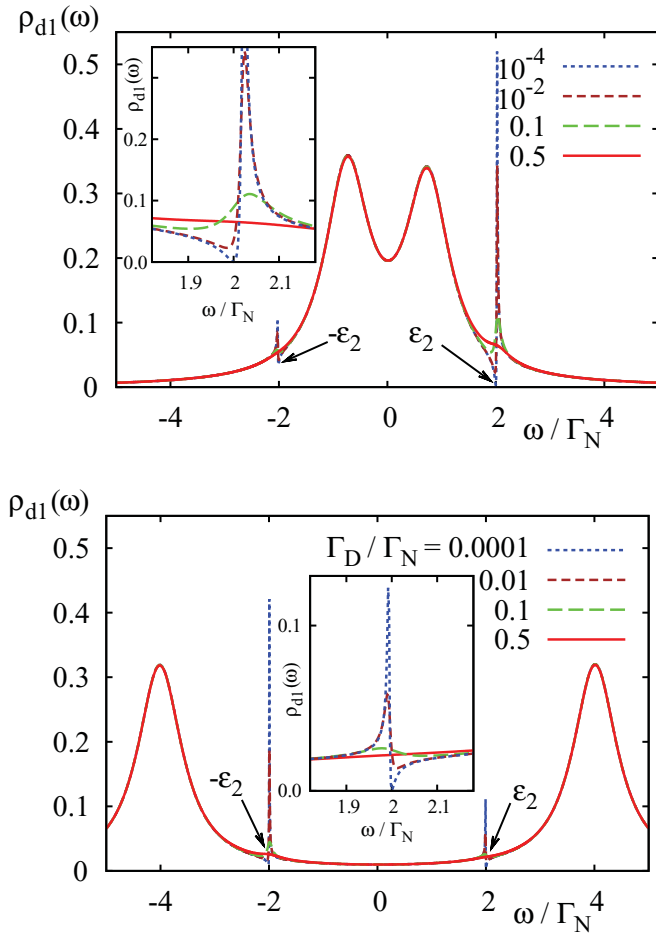


FIG. 3. (Color online) Spectral function $\rho_{d1}(\omega)$ of the central quantum dot in the equilibrium situation. The upper panel corresponds to $\Gamma_S = 1.5\Gamma_N$ (when the quasiparticle energy $E_{d1} < \varepsilon_2$) while the lower one refers to $\Gamma_S = 8\Gamma_N$ (when $E_{d1} > \varepsilon_2$). We used for computations the model parameters $\varepsilon_1 = 0$, $\varepsilon_2 = 2\Gamma_N$, $t = 0.2\Gamma_N$, $U_i = 0$, and several values of Γ_D .

possible.²⁰ In other words, the particle/hole Fano-type line shapes seem to be rather fragile entities with respect to Γ_D . This remark should be taken into account by experimentalists while constructing the double quantum dot structures on a given substrate material.

IV. ANDREEV SPECTROSCOPY

Any practical observation of the interferometric particle/hole Fano line shapes could be detectable only in the tunneling spectroscopy. For this purpose one could measure the differential conductance at small bias (i.e., in the subgap regime $|eV| < \Delta$) when charge transport is provided solely via the anomalous Andreev current $I_A(V)$. Skipping the details we apply here the popular Landauer-type expression

$$I_A(V) = \frac{2e}{h} \int d\omega T_A(\omega) [f(\omega - eV, T) - f(\omega + eV, T)], \quad (14)$$

derived previously in Refs. 31 and 32. The Andreev current depends on occupancy $f(\omega \pm eV, T)$ of the conducting lead

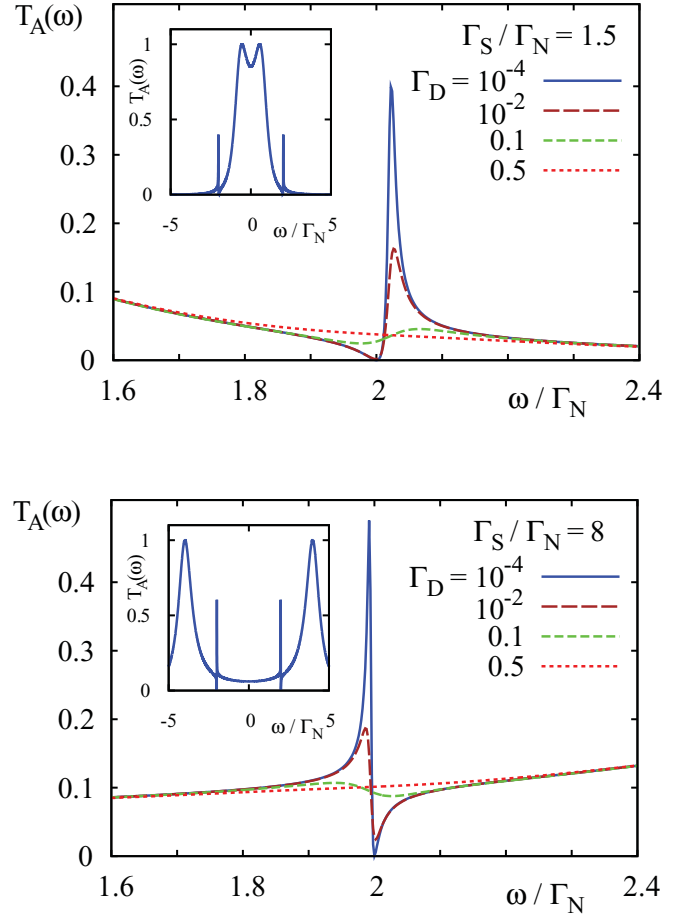


FIG. 4. (Color online) Andreev transmittance $T_A(\omega)$ for the same parameters as in Fig. 3 (Γ_D is expressed in units of Γ_N).

(N) convoluted with the transmittance $T_A(\omega)$. The latter quantity can be determined from the off-diagonal part of the retarded Green's function $G_1(\omega)$ via^{32,33}

$$T_A(\omega) = \Gamma_N^2 |G_{1,12}(\omega)|^2. \quad (15)$$

The Andreev transmittance (15) is a dimensionless quantity and, roughly speaking, it is a measure of the proximity induced on-dot pairing. Of course the transmittance (15) depends indirectly on various structures appearing in the spectrum of the central quantum dot, including the particle-hole Fano features.

In particular, the zero-bias differential conductance

$$G_A(V=0) = \frac{4e^2}{h} \int d\omega T_A(\omega) \left[-\frac{df(\omega, T)}{d\omega} \right] \quad (16)$$

at low temperatures simplifies to

$$G_A(0) = \frac{4e^2}{h} T_A(\omega=0), \quad (17)$$

so the optimal Andreev conductance $4e^2/h$ occurs when $T_A(\omega)$ reaches the ideal value 1. In Fig. 4 we plot ω dependence of the Andreev transmittance for the same set of parameters as discussed in Sec. III. We obtain the symmetric transmittance $T_A(-\omega) = T_A(\omega)$ because anomalous Andreev scattering involves both the particle and hole degrees of freedom. For this reason we notice that at $\omega = \pm\varepsilon_2$ there appear the Fano-type

structures of identical shapes but characterized by an opposite sign of the asymmetry parameter q . Again decoherence proves to have a detrimental influence on both these interferometric structures (compare the curves in Fig. 4 which correspond to several representative values of Γ_D).

V. CORRELATION EFFECTS

Let us now consider additional changes of the Fano line shapes caused by the electron correlations. We shall restrict to the Coulomb repulsion at the side-attached quantum dot U_2 because the effects of U_1 have been already studied previously.¹⁸ Briefly summarizing those studies we can point out that the Coulomb repulsion U_1 leads to the charging effect and (at low temperatures) can induce the narrow Kondo resonance in the spectrum $\rho_{d1}(\omega)$ for $\omega \sim 0$. The latter effect is experimentally manifested by a slight enhancement of the zero-bias Andreev conductance.² Interference effects (originating from the interdot coupling t) would qualitatively affect such a Kondo feature if $\varepsilon_2 \sim 0$. Effects of the Fano interference depend also on the ratio Γ_S/Γ_N controlling efficiency of the induced on-dot pairing which competes with the Kondo physics.³³

So far the correlations have been intensively studied mainly for the case of a single quantum dot coupled between the metallic and superconducting electrodes.¹ For this purpose there have been adopted various many-body techniques, such as the mean-field slave-boson approach,³⁴ noncrossing approximation,³⁵ iterated perturbative scheme,^{30,36} modified slave-boson method,³¹ numerical renormalization-group calculations,³⁷⁻³⁹ and others.^{32,33,40-42} The interest focused predominantly on an interplay between the on-dot pairing and the Kondo state.³⁰ It has been experimentally proved² that such interrelation is governed by the ratio Γ_S/Γ_N . For $\Gamma_S \gg \Gamma_N$ the on-dot pairing plays a dominant role (suppressing or completely destroying the Kondo resonance). In the opposite regime $\Gamma_S \ll \Gamma_N$ the Kondo state is eventually observed (coupling Γ_N to the normal lead is necessary for that).

In this section we study the role of correlations U_2 in the side-coupled quantum dot taking also into account decoherence caused by the floating lead. For simplicity we shall neglect the impact of U_2 on the off-diagonal parts of $\mathbf{G}_2(\omega)$ because the pairing induced in QD₂ for small interdot hopping t can be anyhow expected to be marginal. Thus we determine the Green's function $\mathbf{G}_2(\omega)$ from the Dyson equation (4) imposing the diagonal self-energy

$$\Sigma_2^{e-e}(\omega) \simeq \begin{pmatrix} \Sigma_N(\omega) & 0 \\ 0 & -[\Sigma_N(-\omega)]^* \end{pmatrix}. \quad (18)$$

Formally $\Sigma_N(\omega)$ denotes the self-energy of the Anderson impurity immersed in the normal Fermi liquid. Obviously such self-energy is not known exactly⁴³ therefore we have to invent some approximations.

Among possible choices we adopt the equation of motion method⁴⁴ which is capable to reproduce qualitatively the Coulomb blockade and the Kondo effects. Besides its simplicity this method is, however, not very precise with regard to the low-energy structure of the Kondo peak $\rho_{d2}(\omega \sim 0) =$

$\frac{2}{\pi\Gamma_D} \frac{T_K^2}{\omega^2 + T_K^2}$. Nevertheless our results might give some hints on the qualitative trends and a quality of this information could be improved using more sophisticated tools. Skipping the technicalities discussed by us in Appendix B of Ref. 18 we express the self-energy $\Sigma_N(\omega)$ by

$$[\omega - \varepsilon_2 - \Sigma_N(\omega)]^{-1} = \frac{\tilde{\omega} - \varepsilon_2 - [\Sigma_{N3}(\omega) + U_2(1 - \langle \hat{n}_{2\downarrow} \rangle)]}{[\tilde{\omega} - \varepsilon_2][\tilde{\omega} - \varepsilon_2 - U_2 - \Sigma_{N3}(\omega)] + U_2 \Sigma_{N1}(\omega)}, \quad (19)$$

where $\tilde{\omega} = \omega - \sum_{\mathbf{k}} |V_{\mathbf{k}D}|^2 / (\omega - \xi_{\mathbf{k}D}) \simeq \omega + \frac{i\Gamma_D}{2}$. The other symbols are defined as follows: $\Sigma_{N1}(\omega) = \sum_{\mathbf{k}} |V_{\mathbf{k}D}|^2 f(\xi_{\mathbf{k}D}, T) [(\omega - \xi_{\mathbf{k}D})^{-1} + (\omega - U_2 - 2\varepsilon_2 + \xi_{\mathbf{k}D})^{-1}]$ and $\Sigma_{N3}(\omega) = \sum_{\mathbf{k}} |V_{\mathbf{k}D}|^2 [(\omega - \xi_{\mathbf{k}D})^{-1} + (\omega - U_2 - 2\varepsilon_2 + \xi_{\mathbf{k}D})^{-1}]$. This expression (19) for $\Sigma_N(\omega)$ substituted to the self-energy (18) yields the Green's function $\mathbf{G}_1(\omega)$ of the

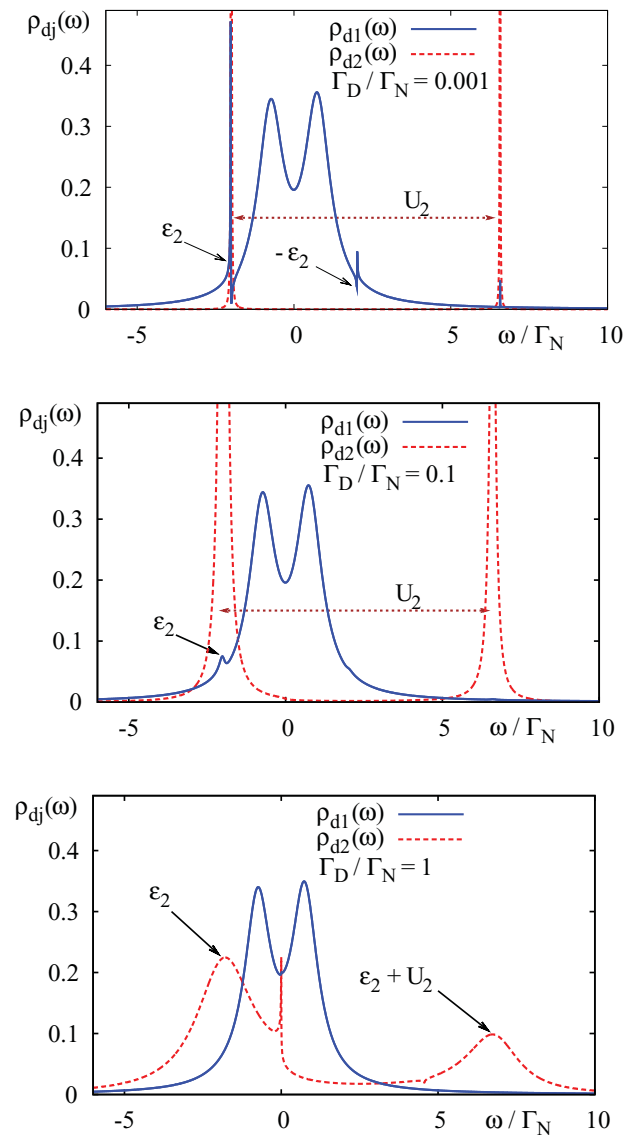


FIG. 5. (Color online) Evolution of the Fano-type line shapes for several couplings Γ_D as indicated. Calculations have been done for $T = 0.001\Gamma_N$ (lower than T_K), using the model parameters $\varepsilon_1 = 0$, $\varepsilon_2 = -2\Gamma_N$, $t = 0.2\Gamma_N$, $\Gamma_S = 1.5\Gamma_N$, and assuming the large superconducting gap $\Delta = 10\Gamma_N$.

central quantum dot via the exact relation (12). In this way we can numerically determine the effect of U_2 on $\rho_{d1}(\omega)$ and on the Andreev transport.

For a weak interdot hopping t (which is necessary to allow for the Fano-type quantum interference) we notice that the correlations U_2 can be manifested in the spectral function $\rho_{d1}(\omega)$ by (i) the charging effect and (ii) another characteristic structure due to the Kondo effect.

(i) The first effect can be observed only if a decoherence is sufficiently weak, strictly speaking for $\Gamma_D \leq 0.1\Gamma_N$. Under such circumstances the particle and hole Fano line shapes (at $\pm\varepsilon_2$) are accompanied by two additional Coulomb satellites at $\pm(\varepsilon_2 + U_2)$. These interferometric features (see the top and middle panels of Fig. 5) are completely washed out from the spectrum when Γ_D slightly exceeds the value $0.1\Gamma_N$. This destructive effect of a decoherence resembles the behavior discussed in Sec. III (see Fig. 3) for the case of uncorrelated quantum dots.

(ii) Instead of the particle/hole Fano line shapes and their Coulomb satellites we can eventually observe a different qualitative structure at $\omega \sim 0$ when the coupling Γ_D is large [provided that temperature $T < T_K(\Gamma_D)$]. Its appearance is related to the Kondo resonance formed at the side-attached quantum dot (see the dashed curve in the bottom panel of Fig. 5). Due to the interdot hopping t the mentioned Kondo resonance affects the central quantum dot in pretty much the same way as did the narrow resonant level ε_2 in a weak-coupling regime Γ_D . Consequently we thus again observe the tiny Fano line shape in the spectral function $\rho_{d1}(\omega)$ of the central quantum dot and in the Andreev transmittance $T_A(\omega)$ near $\omega \sim 0$.

Since the Kondo-induced interferometric structure is hardly noticeable on the large energy scale we show it separately in Fig. 6 restricting to a narrow regime around the Fermi level $\omega = 0$. Let us remark that the Kondo resonance in $\rho_{d2}(\omega)$ and its Fano-type manifestation in $\rho_{d1}(\omega)$ are both very sensitive to temperature. This fact proves that the considered Fano line shape at $\omega \sim 0$ is intimately related to the Kondo effect on the side-attached quantum dot.

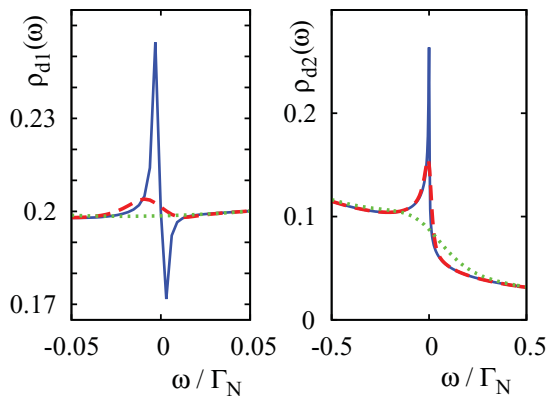


FIG. 6. (Color online) Influence of the Kondo effect appearing in $\rho_{d2}(\omega)$ on a tiny Fano-type structure of the central quantum dot spectrum $\rho_{d1}(\omega)$ near $\omega = 0$. The curves have been calculated using the same parameters as in Fig. 5 for the following temperatures: $T/\Gamma_N = 0.001$ (solid line), 0.01 (dashed line), and 0.1 (dotted line).

VI. CONCLUSIONS

In summary, we have investigated the influence of decoherence and electron correlations on the interferometric Fano-type line shapes of the double quantum dot coupled in T-shape configuration to the conducting and superconducting leads. We find evidence that the decoherence can consequently smear out the Fano line shapes of the particle and hole states. On a microscopic level this detrimental influence can be assigned to a broadening of the resonant levels near $\pm\varepsilon_2$, so that consequently the phase shift of the scattered electron waves is no longer sharp and therefore the Fano-type interference cannot be satisfied.¹⁹

The correlations U_2 on the side-attached quantum dot have the additional qualitative influence. For a weak coupling Γ_D the particle/hole Fano structures at $\pm\varepsilon_2$ are accompanied by the appearance of their Coulomb satellites at $\pm(\varepsilon_2 + U_2)$. All these interferometric features gradually disappear upon increasing Γ_D (i.e., when a dephasing is more effective). On the other hand, in the opposite regime of strong coupling Γ_D , the narrow Kondo resonance appears in the spectral function $\rho_{d2}(\omega)$ of the side-coupled quantum dot. Its formation gives rise to the new interferometric structure appearing in the spectrum of the central quantum dot at $\omega \sim 0$. This temperature-dependent Fano-type line shape is observable in the spectral function $\rho_{d1}(\omega)$ and would be detectable in the Andreev conductance. Such Kondo-induced Fano effect is, however, very tiny, so its experimental verification might be challenging.

ACKNOWLEDGMENTS

We acknowledge useful discussions with B. R. Bułka and K. I. Wysokiński. We are also grateful to M. Büttiker for drawing our attention to Ref. 9, where the idea of a decoherence via the electron phase randomization on the side-attached fermionic reservoir has been introduced. This project was supported by the National Center of Science under Grant No. NN202 263138.

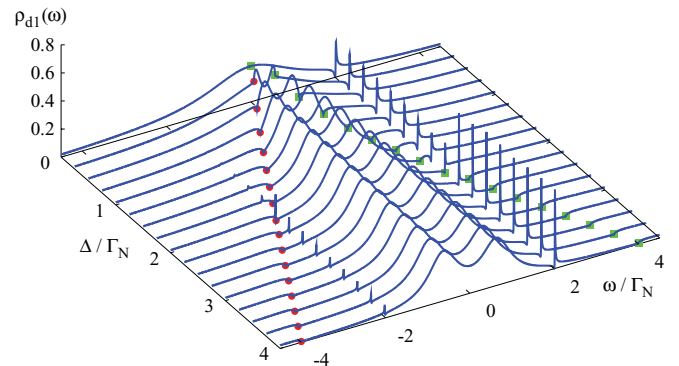


FIG. 7. (Color online) Evolution of the particle/hole Fano line shapes at $\pm\varepsilon_2$ obtained for $\varepsilon_1 = 0$, $\varepsilon_2 = 2\Gamma_N$, $t = 0.2\Gamma_N$, $\Gamma_S = 1.5\Gamma_N$, $U_i = 0$, and for the varying magnitude of Δ . The filled circles and squares indicate the cusplike signatures of the gap edge singularities at $-\Delta$ and $+\Delta$.

APPENDIX: GAP EDGE FEATURES

There is also another important energy scale, relevant for the present study, which is related to a magnitude of the energy gap Δ of superconducting lead. To illustrate its influence on the spectral function $\rho_{d1}(\omega)$ we show in Fig. 7 variation within the region $0 \leq \Delta \leq 4\Gamma_N$. When the energy gap is small we see that the proximity effect is very fragile. For this reason we hardly notice the Fano-type structure at $-\varepsilon_2$ because the

on-dot pairing is rather ineffective. The Fano resonance starts to be well pronounced at $-\varepsilon_2$ when Δ becomes comparable (or larger) than Γ_S . Additionally, the energy gap Δ is responsible for two tiny dips appearing at $\omega = \pm\Delta$. They are signatures of the gap edge singularities of superconducting lead. Roughly speaking, outside the energy regime $|\omega| > \min\{\Delta, \Gamma_S/2\}$ the charge tunneling occurs via the usual single-particle channel and the Andreev tunneling is there no longer dominant.^{31–36}

- ¹A. Martin-Rodero and A. Levy-Yeyati, *Adv. Phys.* **60**, 899 (2011).
- ²R. S. Deacon, Y. Tanaka, A. Oiwa, R. Sakano, K. Yoshida, K. Shibata, K. Hirakawa, and S. Tarucha, *Phys. Rev. Lett.* **104**, 076805 (2010); *Phys. Rev. B* **81**, 121308(R) (2010).
- ³J.-D. Pillet, C. H. L. Quay, P. Morfin, C. Bena, A. Levy-Yeyati, and P. Joyez, *Nat. Phys.* **6**, 965 (2010).
- ⁴R. Maurand, T. Meng, E. Bonet, S. Florens, L. Marty, and W. Wernsdorfer, *Phys. Rev. X* **2**, 011009 (2012).
- ⁵H. I. Jorgensen, K. Grove-Rasmussen, T. Novotny, K. Flensberg, and P. E. Lindelof, *Phys. Rev. Lett.* **96**, 207003 (2006).
- ⁶J. A. van Dam, Yu. V. Nazarov, E. P. A. M. Bakkers, S. De Franceschi, and L. P. Kouwenhoven, *Nature (London)* **442**, 667 (2006).
- ⁷J.-P. Cleuziou, W. Wernsdorfer, V. Bouchiat, T. Ondarucu, and M. Monthieux, *Nat. Nanotech.* **1**, 53 (2006).
- ⁸W.-Z. Gao, W.-J. Gong, Y.-S. Zheng, Y. Liu, and T.-Q. Lü, *Commun. Theor. Phys. (Beijing)* **49**, 771 (2008).
- ⁹M. Büttiker, *IBM J. Res. Dev.* **32**, 63 (1998); *Phys. Rev. Lett.* **57**, 1761 (1986); M. Büttiker and C. A. Stafford, *ibid.* **76**, 495 (1996).
- ¹⁰C. M. Marcus, A. J. Rimberg, R. M. Westervelt, P. F. Hopkins, and A. C. Gossard, *Phys. Rev. Lett.* **69**, 506 (1992); R. M. Clarke, I. H. Chan, C. M. Marcus, C. I. Duruöz, J. S. Harris, K. Campman, and A. C. Gossard, *Phys. Rev. B* **52**, 2656 (1995); H. U. Baranger and P. A. Mello, *ibid.* **51**, 4703 (1995); P. W. Brouwer and C. W. J. Beenakker, *ibid.* **51**, 7739 (1995).
- ¹¹P. W. Brouwer and C. W. J. Beenakker, *Phys. Rev. B* **55**, 4695 (1997).
- ¹²D. S. Golubev, G. Schön, and A. D. Zaikin, *J. Phys. Soc. Jpn., Suppl. A* **72**, 30 (2003).
- ¹³U. Hartmann and F. K. Wilhelm, *Phys. Status Solidi B* **233**, 385 (2002).
- ¹⁴J. Jeske, J. H. Cole, C. Müller, M. Marthaler, and G. Schön, *New J. Phys.* **14**, 023013 (2012).
- ¹⁵R. Žitko, *Phys. Rev. B* **81**, 115316 (2010).
- ¹⁶Y. Tanaka, N. Kawakami, and A. Oguri, *Phys. Rev. B* **78**, 035444 (2008); *J. Phys.: Conf. Ser.* **150**, 022086 (2009).
- ¹⁷Y. Yamada, Y. Tanaka, and N. Kawakami, *J. Phys. Soc. Jpn.* **79**, 043705 (2010); Y. Tanaka, N. Kawakami, and A. Oguri, *Phys. Rev. B* **81**, 075404 (2010).
- ¹⁸J. Barański and T. Domański, *Phys. Rev. B* **84**, 195424 (2011).
- ¹⁹A. E. Miroshnichenko, S. Flach, and Y. S. Kivshar, *Rev. Mod. Phys.* **82**, 2257 (2010).
- ²⁰P. Trocha, *J. Phys.: Condens. Matter* **24**, 055303 (2012).
- ²¹S. Sasaki, H. Tamura, T. Akazaki, and T. Fujisawa, *Phys. Rev. Lett.* **103**, 266806 (2009).
- ²²K. Kobayashi, H. Aikawa, A. Sano, S. Katsumoto, and Y. Iye, *Phys. Rev. B* **70**, 035319 (2004).
- ²³V. Madhavan, W. Chen, T. Jamneala, M. F. Crommie, and N. S. Wingreen, *Phys. Rev. B* **64**, 165412 (2001).
- ²⁴C. Fühner, U. F. Keyser, R. J. Haug, D. Reuter, and A. D. Wieck, *Phys. Rev. B* **66**, 161305 (2002).
- ²⁵P. Stefański, A. Tagliacozzo, and B. R. Buřka, *Phys. Rev. Lett.* **93**, 186805 (2004); W. Hofstetter, J. König, and H. Schoeller, *ibid.* **87**, 156803 (2001); B. R. Buřka and P. Stefański, *ibid.* **86**, 5128 (2001).
- ²⁶A. Grigoriev, J. Sköldberg, G. Wendin, and Z. Crljen, *Phys. Rev. B* **74**, 045401 (2006).
- ²⁷A. R. Schmidt, M. H. Hamidian, P. Wahl, F. Meier, A. V. Balatsky, J. D. Garrett, T. J. Williams, and G. M. Luke, *Nature (London)* **465**, 570 (2010).
- ²⁸L. E. Calvet, J. P. Snyder, and W. Wernsdorfer, *Phys. Rev. B* **83**, 205415 (2011).
- ²⁹H. Q. Hu, *Appl. Phys. Lett.* **78**, 2064 (2001).
- ³⁰Y. Yamada, Y. Tanaka, and N. Kawakami, *Phys. Rev. B* **84**, 075484 (2011).
- ³¹M. Krawiec and K. I. Wysokiński, *Supercond. Sci. Technol.* **17**, 103 (2004).
- ³²Q.-F. Sun, J. Wang, and T.-H. Lin, *Phys. Rev. B* **59**, 3831 (1999); Q.-F. Sun, H. Guo, and T.-H. Lin, *Phys. Rev. Lett.* **87**, 176601 (2001).
- ³³T. Domański and A. Donabidowicz, *Phys. Rev. B* **78**, 073105 (2008); T. Domański, A. Donabidowicz, and K. I. Wysokiński, *ibid.* **78**, 144515 (2008); **76**, 104514 (2007).
- ³⁴R. Fazio and R. Raimondi, *Phys. Rev. Lett.* **80**, 2913 (1998); **82**, 4950 (1999); P. Schwab and R. Raimondi, *Phys. Rev. B* **59**, 1637 (1999).
- ³⁵A. A. Clerk, V. Ambegaokar, and S. Hershfield, *Phys. Rev. B* **61**, 3555 (2000).
- ³⁶J. C. Cuevas, A. Levy Yeyati, and A. Martin-Rodero, *Phys. Rev. B* **63**, 094515 (2001).
- ³⁷Y. Tanaka, N. Kawakami, and A. Oguri, *J. Phys. Soc. Jpn.* **76**, 074701 (2007).
- ³⁸J. Bauer, A. Oguri, and A. C. Hewson, *J. Phys.: Condens. Matter* **19**, 486211 (2007).
- ³⁹T. Hecht, A. Weichselbaum, J. von Delft, and R. Bulla, *J. Phys.: Condens. Matter* **20**, 275213 (2008).
- ⁴⁰S. Y. Cho, K. Kang, and C.-M. Ryu, *Phys. Rev. B* **60**, 16874 (1999).
- ⁴¹Y. Avishai, A. Golub, and A. D. Zaikin, *Phys. Rev. B* **63**, 134515 (2001); T. Aono, A. Golub, and Y. Avishai, *ibid.* **68**, 045312 (2003).
- ⁴²V. Koerting, B. M. Andersen, K. Flensberg, and J. Paaske, *Phys. Rev. B* **82**, 245108 (2010).
- ⁴³A. C. Hewson, *The Kondo Problem to Heavy Fermions* (Cambridge University Press, Cambridge, England, 1993).
- ⁴⁴H. Haug and A.-P. Jauho, *Quantum Kinetics in Transport and Optics of Semiconductors* (Springer-Verlag, Berlin, 1996).